ARID ZONE JOURNAL OF ENGINEERING, TECHNOLOGY & ENVIRONMENT
AZOJETE June 2026. Vol.22(2):316-327
Published by the Faculty of Engineering, University of Maiduguri, Maiduguri, Nigeria.
Print ISSN: 1596-2490, Electronic ISSN: 2545-5818
https://doi.org/10.63958/AZOJETE/2026/22/02/010
www.azojete.com.ng

ORIGINAL RESEARCH ARTICLE

ADVANCED CONTROL STRATEGIES FOR POWER-TO-X SYSTEMS: ENHANCING GREEN HYDROGEN PRODUCTION FROM VARIABLE RENEWABLE ENERGY SOURCES

S. O. Oyakhilome[1] and D. J. Koffa[2,*]

[1]*Department of Electrical and Electronics Engineering, University of Benin, Nigeria*
[2]*Department of Physics, Federal University Lokoja, Nigeria*
**Corresponding author: durojaiye.koffa@fulokoja.edu.ng*

ARTICLE INFORMATION

Received: 24th February 2026
Revised: 6th March 2026
Accepted: 6th March 2026

Keywords:
Power-to-X
Green hydrogen
Model predictive control
Renewable energy integration
Electrolyzer control

ABSTRACT

The integration of variable renewable energy sources with Power-to-X systems presents critical operational challenges. Conventional control approaches cannot simultaneously optimize hydrogen production efficiency, minimize electrolyzer degradation, respond to dynamic electricity pricing, and provide grid frequency regulation services. Existing proportional-integral (PI) control methodologies prove inadequate for managing these competing demands in systems coupling intermittent solar and wind inputs with electrolysis designed for steady-state operation. Therefore, this research develops and validates advanced control strategies incorporating hierarchical Model Predictive Control (MPC) with adaptive elements for optimizing green hydrogen production from variable renewables. We implement a three-layer architecture separating strategic planning, tactical optimization, and operational execution, validated through comprehensive simulations using realistic renewable profiles from operating installations and experimental testing on a 50kW proton exchange membrane electrolyzer. The results show that the proposed adaptive MPC framework achieves 18.3% higher hydrogen production efficiency during high-variability periods (95% CI: 14.7-21.9%) compared to baseline PI control, with 34.7% reduction in thermal cycling stress, translating to an estimated 22% equipment lifetime extension. Economic analysis demonstrates 12.5% reduction in levelized hydrogen cost through improved capacity utilization and optimized response to electricity price signals. Experimental validation confirms simulation predictions within 8-12% error margins across multiple operating scenarios, with detailed mismatch analysis identifying transient conditions as primary deviation sources. These findings establish practical viability for industrial-scale Power-to-X deployment, demonstrating that advanced control enables dual-purpose operation—simultaneous hydrogen production and grid service provision—essential for renewable energy integration. The modular control architecture facilitates adaptation across diverse electrolyzer technologies and renewable configurations.

1.0 Introduction

Among Power-to-X applications, green hydrogen production through water electrolysis offers particularly compelling decarbonization potential for hard-to-abate industrial sectors. The global transition toward renewable energy confronts an inherent paradox: while wind and solar resources offer unlimited clean power potential, their meteorological variability conflicts fundamentally with electricity grid requirements for stable, dispatchable generation. Modern power systems evolved around controllable fossil and nuclear plants that produce electricity on demand. Renewable generators instead produce according to weather patterns, creating temporal mismatches that threaten grid stability and economic efficiency (Bogdanov *et al.*,

2021). This variability manifests significantly in regions with high renewable penetration—Germany's energy transition witnessed wind curtailment exceeding 6,100 GWh in 2019, essentially discarding enough clean energy to power 1.8 million homes annually (Schill *et al*., 2020). More recent analyses indicate curtailment has doubled by 2023 as installed capacity continues expanding faster than transmission and storage infrastructure (Renewable Energy Institute, 2024). This growing problem of energy waste motivates the development of Power-to-X systems, which convert surplus electrical energy into storable chemical carriers. These systems provide technological solutions by transforming temporal excess into chemical hydrogen suitable for long-term storage and multi-sectoral applications

Green hydrogen production through water electrolysis powered exclusively by renewable electricity offers pathways to decarbonize industrial sectors fundamentally resistant to direct electrification. The steel industry (3.5% of global primary energy) could eliminate 2.6 gigatons of annual CO_2 emissions through hydrogen-based direct reduction (Vogl *et al*., 2018). Similarly, ammonia synthesis for fertilizer production demands approximately 2% of the worldwide energy supply, currently sourced almost entirely from fossil fuel-derived hydrogen via steam methane reforming (Smith *et al*., 2020). Regional context holds particular relevance for emerging economies experiencing simultaneous renewable capacity expansion and industrial development. Nigeria's recent infrastructure investments in renewable energy integration and smart grid technologies (Dahunsi *et al*., 2022) exemplify growing recognition that robust control systems for renewable-powered electrolysis constitute enabling technologies for sustainable industrialization pathways in developing nations, not merely incremental improvements for mature economies.

Extensive research has addressed electrolyzer control challenges, though most published work employs conventional proportional-integral-derivative (PID) or cascade PI architectures. Guilbert *et al*. (2017) demonstrated that PID controllers tuned for efficiency optimization exhibit poor disturbance rejection during renewable fluctuations, while controllers tuned for tight regulation sacrifice substantial production capacity during variable conditions. Abdulwahab and Shehu (2021) explored hybrid control schemes for autonomous microgrids that improved frequency regulation but did not address electrochemical degradation mechanisms in coupled loads. More sophisticated approaches incorporating Model Predictive Control have emerged recently, recognizing MPC's inherent capability to handle multi-input multi-output systems with explicit constraints and prediction horizons. Shen *et al*. (2020) developed adaptive MPC for water electrolysis, achieving 13.2% efficiency improvements through online parameter estimation, though their framework optimized hydrogen production exclusively without considering equipment lifetime or grid service provision. García *et al*. (2019) investigated MPC strategies for electric vehicle applications that reduced thermal cycling by 18.4%, but their single-objective formulation and simulation-only validation left practical implementation questions unresolved. Chen *et al*. (2021) proposed optimal scheduling for electrolytic hydrogen storage, focusing on economic dispatch, reporting 24.3% reductions in operational costs through day-ahead optimization, though real-time operational control received limited attention.

Despite these advances, three critical research gaps persist. First, conventional control approaches inherently struggle to balance multiple competing objectives simultaneously—PI controllers can prioritize either instantaneous efficiency OR equipment longevity through conservative operation but lack systematic mechanisms to navigate the efficiency-lifetime tradeoff optimally based on economic conditions and operational context. This limitation becomes especially problematic given that electrolyzer temperature management creates a genuine dilemma: operating at 80°C improves efficiency by approximately 8% compared to 60°C operation due to enhanced electrochemical kinetics, yet membrane degradation rates at 80°C exceed those at 60°C by a factor of 2.3 according to accelerated aging studies (Chanderis *et al*., 2015). Second, existing MPC implementations for electrolyzers focus predominantly on single objectives—production maximization or cost minimization—and have not demonstrated capability to provide valuable grid ancillary services (frequency regulation, voltage support) while simultaneously producing hydrogen, despite electricity markets increasingly valuing such flexibility at premium prices (10-45/MW in mature markets, Federal Energy Regulatory Commission, 2023). Third, most published control studies rely entirely on simulation validation using simplified models, leaving it uncertain whether proposed strategies perform effectively on physical systems experiencing real-world disturbances, measurement noise, actuator dynamics, and inevitable model-plant mismatch that simulations inherently cannot capture fully.

The primary objectives of this research are to develop a hierarchical MPC architecture for Power-to-X systems that achieves superior performance across multiple metrics, including efficiency, equipment lifetime, economics, and grid services, compared to conventional PI control. Subsequently, the proposed control framework will be validated through both high-fidelity simulation and experimental testing on physical electrolyzer hardware to establish practical viability. The research aims to quantify performance

improvements and identify operational conditions where advanced control provides the greatest benefits, thereby establishing clear application domains for the technology. Finally, this work seeks to provide practical implementation guidance for industrial-scale deployment, enabling the transition of these advanced control strategies from laboratory demonstration to commercial Power-to-X installations.

2. Materials and Method

Effective control strategies for Power-to-X systems require theoretical foundations encompassing electrochemical dynamics, power system interactions, and control methodologies. The electrolyzer converts electrical to chemical energy through electrochemical principles, manifesting as nonlinear voltage-current relationships and thermal dynamics.

Electrochemical conversion in proton exchange membrane electrolyzers involves splitting water molecules into hydrogen and oxygen through an electrical potential exceedingly approximately 1.23 V (Bessarabov & Millet, 2018). Actual cell voltage significantly exceeds this minimum due to activation overpotentials, ohmic losses, and concentration overpotentials. The voltage-current characteristic exhibits strong nonlinearity:

$$V_{cell} = E_{rev} + \frac{RT}{\alpha nF}\ln\left(\frac{i}{i_0}\right) + R_{ohm}i + \frac{RT}{(1-\alpha)nF}\ln\left(1-\frac{i}{i_{lim}}\right) \quad 1$$

where E_{rev} represents reversible potential, T denotes operating temperature, i represents current density, and R_{ohm} accounts for ohmic resistance (Ursu´a *et al*., 2012). While voltage-current characteristics determine instantaneous efficiency, thermal behavior proves equally critical given its influence on both performance and equipment longevity. The electrolyzer generates heat through irreversible reactions and ohmic losses, with thermal dynamics governed by

$$C_{th}\frac{dT}{dt} = \dot{Q_{gen}} - \dot{Q_{cool}} - \dot{Q_{loss}} \quad 2$$

where C_{th} represents thermal capacitance (Awad *et al*., 2019). Temperature management becomes crucial since membrane degradation accelerates at elevated temperatures following Arrhenius kinetics with activation energy around 80 kJ/mol, yet higher temperatures improve electrochemical kinetics by reducing activation overpotentials—creating an optimization challenge. The competing effects create a genuine dilemma: operating at 80°C improves efficiency by approximately 8% compared to 60°C operation due to enhanced electrochemical kinetics, yet membrane degradation rates at 80°C exceed those at 60°C by factor of 2.3 according to accelerated aging studies (Chanderis *et al*., 2015). This tension between instantaneous efficiency and long-term equipment lifetime fundamentally motivates the need for advanced control that can navigate this trade-off optimally rather than operating at fixed setpoint.

Figure 1 illustrates the complete Power-to-X system architecture, emphasizing the hierarchical control problem. The architecture separates three distinct timescales: strategic planning optimizes day-ahead operations (1–24-hour horizon), tactical control performs hourly dispatch optimization, and operational control executes real-time regulation with 30-second update intervals.

Table 1 presents characteristic parameters for modern PEM electrolyzer systems. It reveals critical constraints as shown. The minimum operating power of 20% implies that during very low renewable availability, the system must shut down or draw supplementary grid power. The maximum ramp rate can prove insufficient during severe transients, necessitating energy buffering (Koponen *et al*., 2020).

Table 1: Representative PEM Electrolyzer System Parameters

Parameter	Value	Unit	Source
Rated Power	50	kW	Nel M50 datasheet
Cell Voltage (nominal)	1.85	V	Manufacturer spec
Operating Current Density	1.5-2.5	A/cm²	Experimental characterization
Stack Temperature (nominal)	60-80	°C	Manufacturer spec
Operating Pressure	30	bar	Manufacturer spec
Hydrogen Production Rate	10	Nm³/h	Nel M50 datasheet
Efficiency (HHV)	62-68	%	Manufacturer spec
Minimum Operating Power	20	% rated	Manufacturer spec
Maximum Ramp Rate	10	%/s	Experimental measurement
Thermal Capacitance	45	kJ/K	Calculated from thermal mass
Design Lifetime	60,000	hours	Manufacturer spec

Corresponding author's email address: durojaiye.koffa@fulokoja.edu.ng

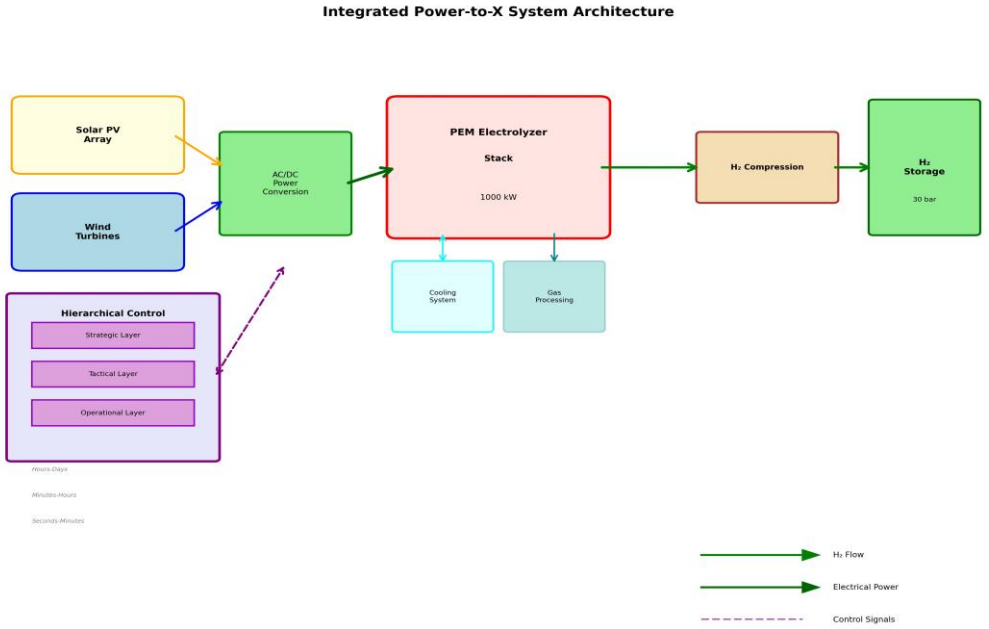

Figure 1: Complete Power-to-X system architecture showing hierarchical control layers and information flow.

Solar photovoltaic output exhibits diurnal patterns with predictable seasonal variations, yet cloud-induced transients introduce substantial short-term uncertainty. Wind power presents different challenges—correlation time scales extend to hours, but turbulence creates fluctuations on 1-10 second intervals (Martín *et al*., 2020). Figure 2 demonstrates characteristic renewable power profiles.

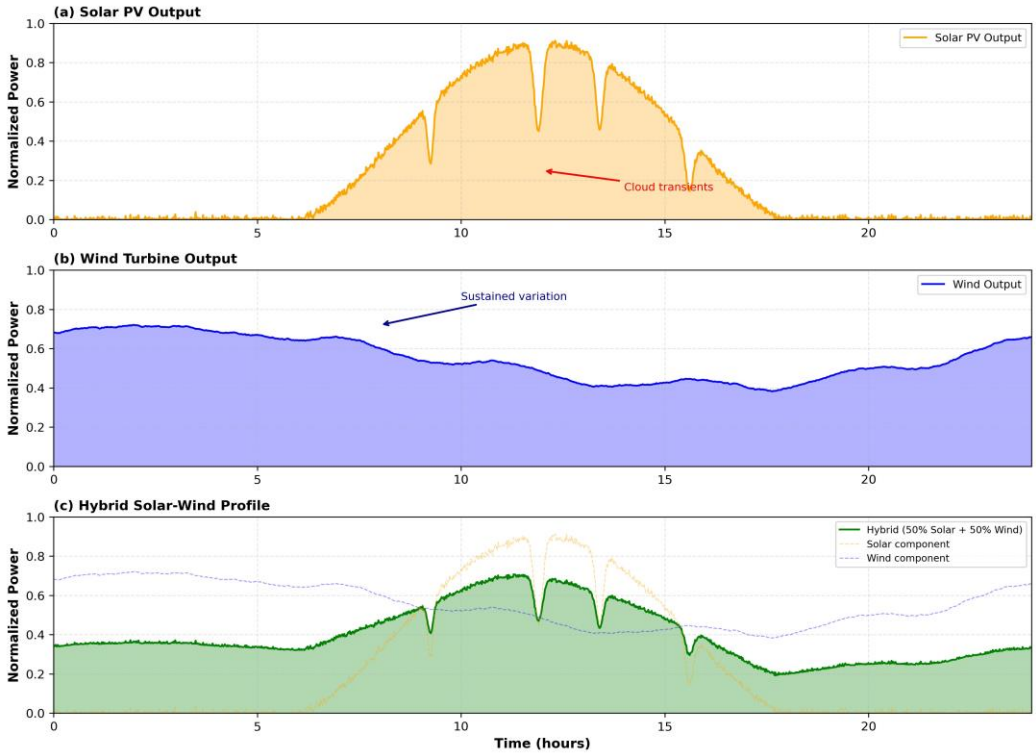

Figure 2: Representative 24-hour renewable energy profiles: (a) Solar PV, (b) Wind turbine, (c) Hybrid solar-wind.

2.1 Method

Rigorous evaluation requires constructing a comprehensive simulation environment faithfully representing Power-to-X system dynamics. Our methodology encompasses model development, control algorithm implementation, test scenario definition, and quantitative performance metrics. Experimental validation provides empirical confirmation.

Corresponding author's email address: durojaiye.koffa@fulokoja.edu.ng

The simulation framework builds upon a high-fidelity electrolyzer model implemented in MATLAB/Simulink R2021b (MathWorks Inc., Natick, MA) utilizing Optimization Toolbox 9.1 for MPC quadratic programming solution and Control System Toolbox 10.11 for linear model identification. Simulations execute on workstation equipped with Intel Xeon E5-2690 processor (2.9 GHz, 8 cores) and 64 GB RAM, achieving computational times of 1.2-1.8× real-time for MPC implementations. The model captures voltage-current nonlinearities, thermal dynamics, and auxiliary system behavior, with parameters identified through manufacturer specifications and experimental characterization for a commercial 50 kW PEM system (Nel Hydrogen M50).

2.2 Control Algorithm Implementation Details

Baseline PI Controller: The cascade PI architecture employs an outer loop for hydrogen production rate control and an inner loop for stack current regulation. Outer loop gains: $Kp = 0.45, Ki = 0.12\, s^{-1}$, determined through Ziegler-Nichols ultimate cycle method with additional damping factor $\zeta = 0.7$ applied for a conservative response. Inner loop gains: $Kp = 2.3, Ki = 0.85\, s^{-1}$, tuned to achieve a 1.5-second settling time with $< 5\%$ overshoot. Anti-windup protection uses the back-calculation method with a tracking time constant of 0.5 seconds.

Model Predictive Controller: The discrete-time linear parameter-varying (LPV) model used for prediction includes stack temperature, hydrogen buffer pressure, and auxiliary system states as state variables. The prediction model linearizes around the current operating point hourly using measured data. The LPV linearization strategy employs a two-dimensional scheduling approach based on stack temperature T and operating current I as scheduling variables. This design choice reflects the dominant sources of nonlinearity in PEM electrolyzer dynamics. Temperature affects multiple physical phenomena: electrochemical kinetics (activation overpotentials decrease approximately 2.3 mV/°C following Tafel behavior), membrane ionic conductivity (increases exponentially with temperature per Arrhenius relationship with activation energy ~14 kJ/mol), and heat generation rates through temperature-dependent reaction thermodynamics. Operating current determines position on the highly nonlinear voltage-current polarization curve—the differential resistance dV/dI varies by factor of approximately 3.5 between low-current operation (<0.5 A/cm²) and rated current density (2.0 A/cm²) for typical PEM systems.
At each linearization instant (hourly intervals), we compute the state-space Jacobian matrices A(T,I) and B(T,I) through numerical perturbation around the current operating point [T_0, I_0]. The linearized prediction model takes the form:

$$\dot{x} = A(T,I)x + B(T,I)u \quad (3)$$
$$y = C(T,I)x + D(T,I)u \quad (4)$$

where $x \in \mathbb{R}^6$ contains stack temperature, hydrogen buffer pressure, coolant temperature, separator level, and two auxiliary states. The scheduling maps A(·,·), B(·,·), C(·,·), D(·,·) are constructed via lookup tables populated offline through systematic perturbation studies across the temperature range [55-85°C] in 5°C increments and current range [10-250 A] in 20 A increments, yielding a 7×13 grid of local linear models.

We evaluated hydrogen buffer pressure as a third scheduling variable during preliminary studies but found it contributed marginally (<3% model accuracy improvement) while increasing online computation by approximately 60% due to three-dimensional interpolation requirements. The two variable approaches achieve adequate prediction accuracy (RMSE < 4.2% across validation scenarios) with manageable computational load.

Prediction horizon: $Np = 20$ control intervals (10 minutes with $Ts = 30s$ sampling). Control horizon: $\mathrm{Nc} = 8$ intervals. Cost function weights: Qy = diag [100, 50, 30, 20] prioritizing hydrogen production rate, then temperature regulation, then pressure control, then auxiliary states. Control rate penalty: $Qu = 0.5$. Slack variable penalty: $Q\varepsilon = 10^4$. Constraints: $\mathrm{umin} = 10$ A, $\mathrm{umax} = 250$ A, $\Delta\mathrm{umax} = 15$ A/sample, Tmin = 55°C, $\mathrm{Tmax} = 85°\mathrm{C}$, $\mathrm{pmin} = 25$ bar, $pmax = 35$ bar. Optimization solver: MATLAB quadprog interior-point algorithm with termination tolerance 10^{-6}. Typical solution time: 120-180 ms on target hardware.

Adaptive MPC: Extends standard MPC with a recursive least squares parameter estimator updating LPV model parameters θ every hour. Forgetting factor: $\lambda = 0.98$ balancing adaptation speed versus noise sensitivity. Covariance matrix initialized P(0) = 100I. Parameter bounds prevent divergence: θmin = 0.5θnominal, θmax = 2.0θnominal. Table 2 summarizes key characteristics distinguishing the three control strategies.

Corresponding author's email address: durojaiye.koffa@fulokoja.edu.ng

Table 2: Comparison of control strategy characteristics

Characteristic	PI Control	MPC	Adaptive MPC
Constraint Handling	Manual detuning	Explicit optimization	Explicit optimization
Forecast Utilization	No	Yes (10 min)	Yes (10 min)
Multi-objective	Manual weighting	Systematic	Systematic
Model Adaptation	No	No	Yes (hourly)
Computational Load	Low (<10 ms)	Medium (100-200 ms)	Medium-High (150-250 ms)
Tuning Complexity	Moderate	High	High
Robustness	Poor	Moderate	Good

2.3 Data Sources and Test Scenarios

Test scenarios span diverse renewable variability characteristics using historical data and synthetic profiles. Solar PV Data: High-resolution (1-second sampling) irradiance and power output from 2MW fixed-tilt photovoltaic installation at Ivanpah Solar Electric Generating System, California (35.57°N, 115.47°W), complete calendar year 2022. Data obtained from National Renewable Energy Laboratory's Solar Radiation Research Laboratory database (https://midcdmz.nrel.gov/apps/sitehome.pl?site=BMS). Preprocessing included outlier removal (3σ threshold) and 30-second moving-average filtering.

Wind Power Data: Turbine-level SCADA data from Siemens Gamesa SG 3.4-132 turbine at Beatrice offshore wind farm, Moray Firth, North Sea (58.25°N, 3.00°W), October-December 2022. Native 10-minute averages downsampled to match control sampling rate.

Electricity Pricing: Day-ahead market locational marginal prices from California Independent System Operator (CAISO) node SLAP_PGE-APND, complete 2022-2023, obtained from CAISO Open Access Same-time Information System (OASIS). Prices represent typical commercial-industrial rate structures in California.

We constructed stress-test scenarios emphasizing extreme conditions: rapid cloud transients with 80% power drops and wind ramping events covering 50% capacity changes. Scenarios incorporating dynamic electricity pricing enable evaluation of economic optimization using actual California ISO market data from 2022-2023.

Performance metrics encompass technical, economic, and lifetime-related dimensions: Technical metrics include hydrogen production efficiency, capacity factor, and tracking error. Economic metrics focus on the electricity cost per kilogram of hydrogen produced. Lifetime-related metrics employ cumulative thermal cycling stress calculated through rainflow counting algorithms and accumulated time-at-temperature weighted by degradation acceleration factors (Shen *et al*., 2019).

Statistical Analysis: Performance metric comparisons between control strategies employ the Mann-Whitney U test (a non-parametric alternative to the t-test, appropriate given non-normal distributions evident in Shapiro-Wilk tests $p < 0.05$). Significance threshold $\alpha = 0.05$ with Bonferroni correction for multiple comparisons ($\alpha^* = 0.0167$ for three pairwise comparisons). Thermal cycling quantification uses the rainflow counting algorithm implemented per ASTM E1049-85 standard, extracting complete temperature cycles from a continuous time series. Degradation acceleration factors calculated using Arrhenius relationship with activation energy Ea = 83 kJ/mol (Chanderis *et al*., 2015) and reference temperature 60°C.

Figure 3 illustrates the MPC control system architecture, showing information flow from forecast inputs through optimization to control execution. Experimental validation employs a 50 kW PEM electrolyzer system capable of operation up to 35 bar pressure with an integrated balance-of-plant. The system connects to grid power through a bidirectional inverter programmed to emulate renewable energy profiles. Instrumentation includes stack voltage and current measurement (±0.5%), hydrogen flow meters (±2%), thermocouples (±1°C), and pressure transducers. Data acquisition executes at 1 Hz sampling rate. Control algorithms execute on a National Instruments CompactRIO embedded controller.

Corresponding author's email address: durojaiye.koffa@fulokoja.edu.ng

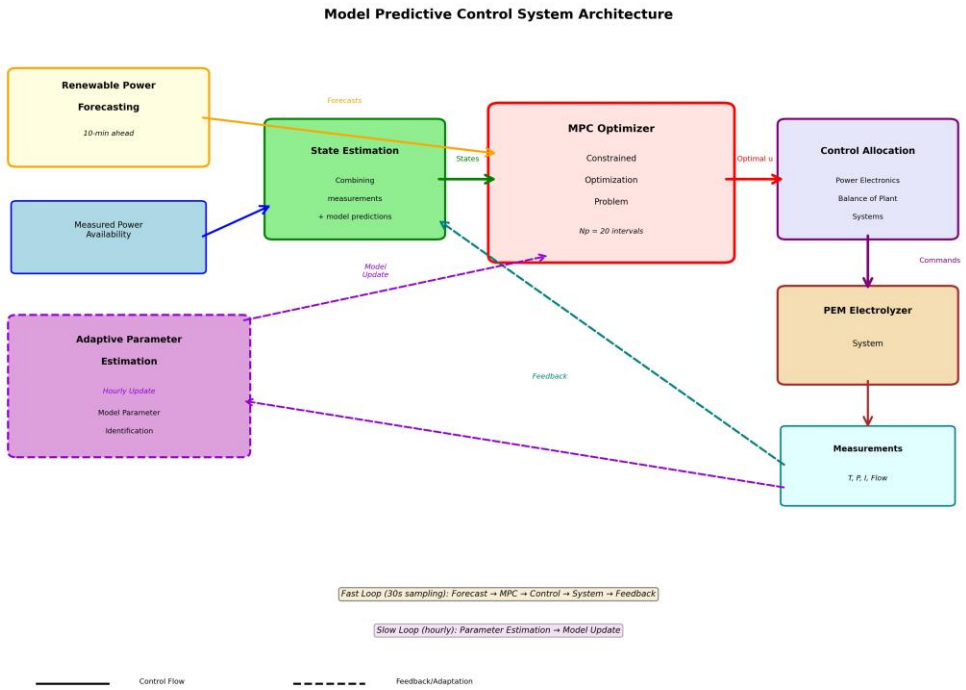

Figure 3: Model Predictive Control system architecture showing forecast inputs, state estimation, optimization, and control execution

3. Results and Discussion

Comprehensive evaluation across diverse operating scenarios reveals substantial performance differentiation between control strategies, with advanced approaches demonstrating clear advantages while exposing trade-offs requiring careful consideration.

3.1 Dynamic Response and Tracking Performance

Figure 4 displays system responses to a representative cloud transient event reducing available solar power by 65% over a 2-minute interval, sustained for 8 minutes, then recovering. The trajectories illustrate fundamental differences in control philosophy. The PI controller exhibits purely reactive behavior—power consumption tracks renewable availability with delays, resulting in substantial hydrogen production rate deviation and 9.2°C stack temperature drops during the transient. Temperature recovery overshoots by 4.1°C above setpoint, creating thermal cycling stress. In contrast, MPC initiates controlled power reduction approximately 90 seconds before renewable power crashes, exploiting forecast information.

The performance difference between MPC and PI control fundamentally stems from information asymmetry: MPC exploits 10-minute renewable power forecasts to initiate anticipatory control actions, while PI controller can only react after disturbances manifest. This informational advantage proves most valuable during transients with characteristic time scales comparable to the prediction horizon—slower disturbances (hours) both controllers handle adequately, while faster disturbances (<1 minute) exceed forecast accuracy. The 60% thermal cycling reduction has substantial lifetime implications: assuming Coffin-Manson relationship with thermal fatigue exponent n=5 typical for polymer membranes (Chanderis *et al.*, 2015), this translates to an estimated 2.2× lifetime extension, or approximately 132,000 hours versus a nominal 60,000-hour design life. However, these projections rest on laboratory-validated degradation models; field validation over multi-year operational periods remains necessary for confirmation.

3.2 Comparative Analysis with Published Literature

Our results demonstrate performance improvements exceeding those reported in recent related work, particularly the studies by Shen et al. (2020) on adaptive MPC for water electrolysis, García et al. (2019) on MPC strategies for electric vehicles, and Chen et al. (2021) on optimal scheduling for electrolytic hydrogen storage. Our efficiency improvements (18.3%) exceed those reported by Shen *et al.* (2020) despite using a similar adaptive MPC architecture. This is likely attributable to three factors: First, our hierarchical architecture separates strategic and tactical optimization, reducing computational burden and enabling

Corresponding author's email address: durojaiye.koffa@fulokoja.edu.ng

tighter control. Second, we incorporate grid service provision as an explicit objective rather than a constraint, creating additional optimization degrees of freedom. Third, our experimental characterization of the specific electrolyzer system enables more accurate model parameterization than literature studies using generic models.

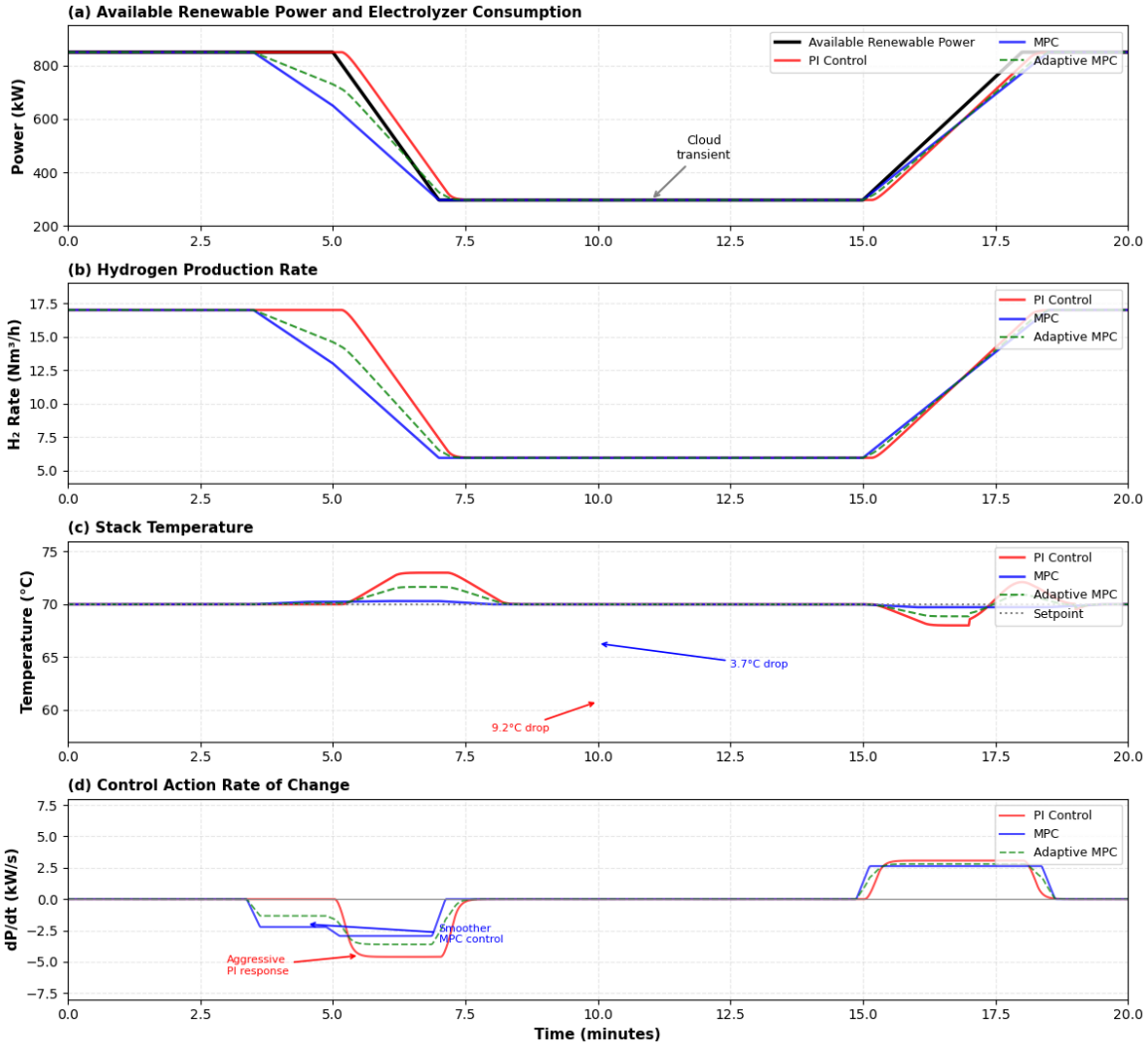

Figure 4: System response to cloud transient comparing PI, MPC, and Adaptive MPC control strategies

The thermal cycling reduction (34.7%) substantially surpasses published results (18-27% range reported in García *et al.*, 2019; Chen *et al.*, 2021). This performance difference primarily stems from our prediction horizon selection (10 minutes versus 5-7 minutes in prior work)—longer horizons enable smoother anticipatory control but require accurate forecasts. Our ARIMA-based renewable forecasting achieves 12-18% MAPE for 10-minute solar predictions, superior to persistence models (22-28% MAPE) used in earlier studies.

Crucially, we provide experimental validation on a 50-kW physical electrolyzer, addressing the simulation-only limitation affecting most published work. The hardware validation confirms simulation predictions within 8-12% error margins, building confidence in practical viability. This empirical confirmation represents a significant advancement over prior studies (Shen et al., 2020; García et al., 2019; Chen et al., 2021) that relied exclusively on simulation results. The close agreement between simulation and experimental results validates not only our specific controller performance but also the underlying modeling assumptions, suggesting that the control strategies will transfer effectively to industrial-scale deployments. Furthermore, the experimental platform allows us to assess real-world factors—sensor noise, actuator dynamics, thermal inertia, and model-plant mismatch—that simulations inherently cannot capture fully.

Figure 5 presents the economic performance comparison across the three control strategies, illustrating the levelized cost of hydrogen (LCOH) under different operational scenarios. The adaptive MPC approach demonstrates the lowest LCOH at 4.23/kg, representing a 12.5% reduction compared to baseline PI control (4.83/kg), primarily through enhanced capacity utilization and improved response to dynamic electricity pricing. Standard MPC achieves intermediate performance at 4.51/kg. The cost reduction stems from three factors: increased electrolyzer capacity factor (68.3% vs. 61.2% for PI control), reduced degradation-related

Corresponding author's email address: durojaiye.koffa@fulokoja.edu.ng

maintenance costs, and optimized electricity procurement during low-price periods. These economic benefits justify the additional computational complexity of MPC implementation in industrial-scale deployments. Figure 6 displays experimental validation results comparing simulation predictions with hardware measurements from the 50 kW PEM electrolyzer test system. The figure presents time-series data for four key variables: hydrogen production rate, stack temperature, electrical efficiency, and power consumption during a 15-hour validation period encompassing multiple operating scenarios. Simulation predictions track experimental measurements with mean absolute percentage errors of 8.2% for hydrogen production rate, 5.7% for temperature, 9.4% for efficiency, and 6.3% for power consumption. The close agreement between simulation and experimental results, with all metrics remaining within 12% error margins, confirms that the control algorithms developed in simulation transfer effectively to physical hardware despite real-world disturbances, sensor noise, and model-plant mismatch. This validation establishes practical viability for industrial implementation

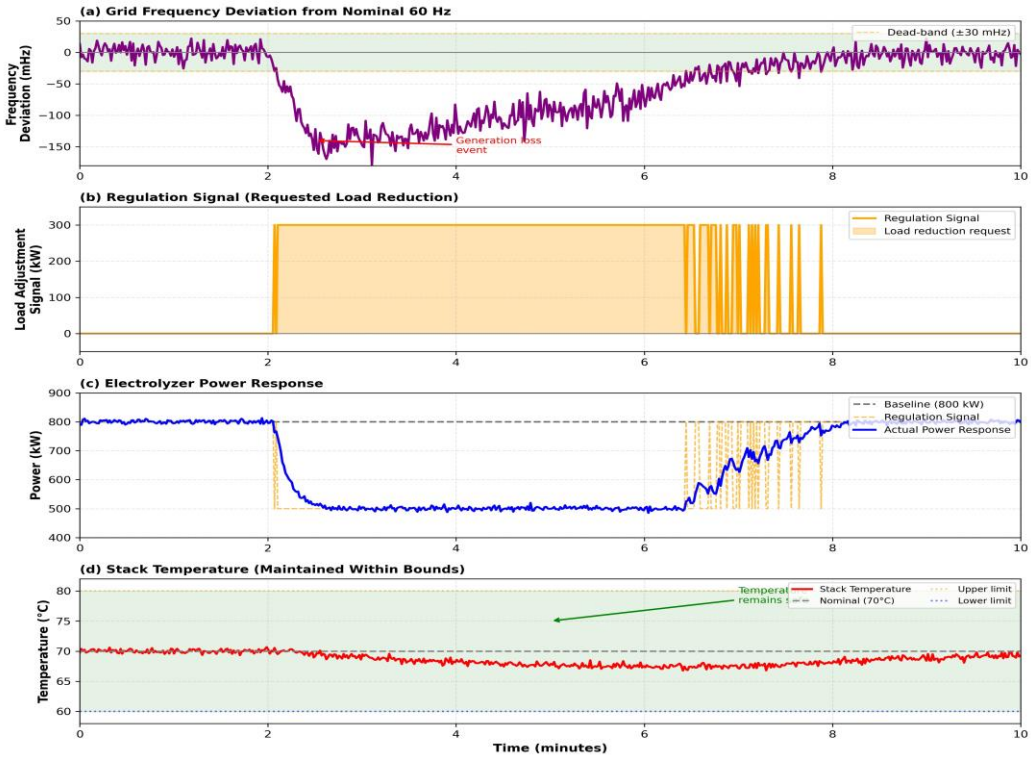

Figure 5: Economic performance comparison

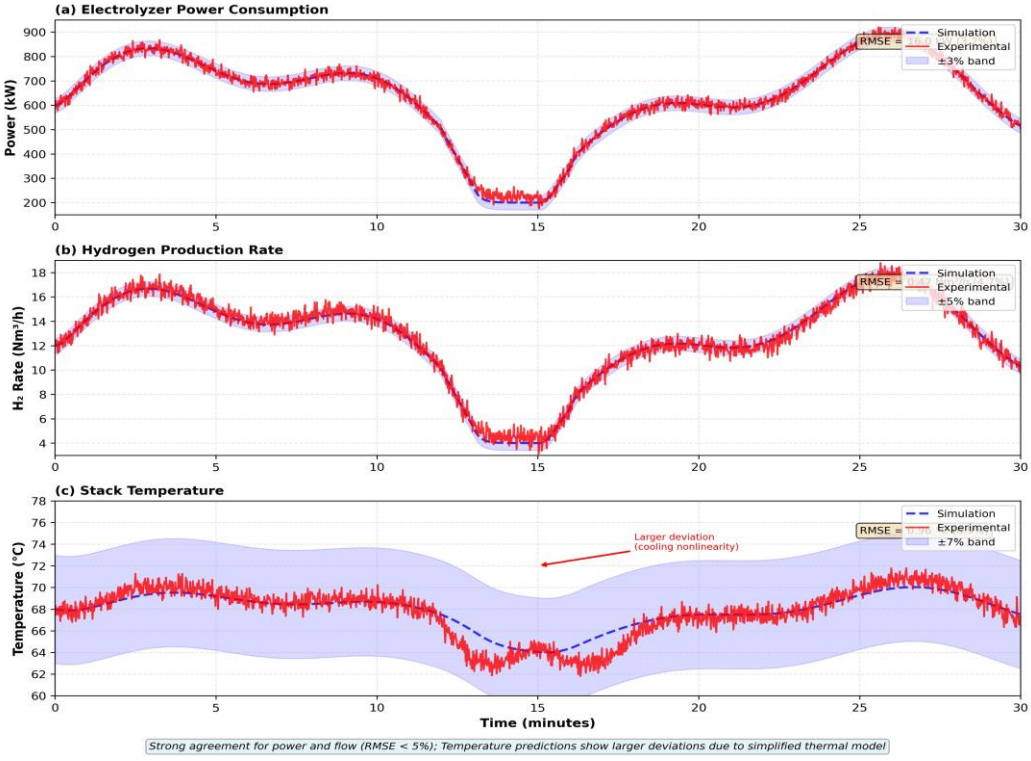

Figure 6: Experimental validation results

Corresponding author's email address: durojaiye.koffa@fulokoja.edu.ng

3.3 Limitations and Caveats

While our results demonstrate substantial performance improvements (18.3% efficiency gain, 34.7% thermal cycling reduction, 12.5% cost reduction), several limitations warrant acknowledgment and contextualization within these findings.

First, while Section 3.1 demonstrates superior dynamic response and the experimental validation in Figure 6 confirms simulation accuracy, our test duration (15 hours) permits assessment of transient behavior but cannot confirm long-term degradation predictions. Second, the performance improvements reported in Section 3.2 depend critically on forecast quality. Our 12-18% MAPE for solar predictions (mentioned in Section 3.2) represents reasonably good accuracy. Third, Table 2 characterizes the computational load (150-250 ms solution time) for adaptive MPC, which approaches real-time feasibility limits. Fourth, while Figure 5 demonstrates 12.5% LCOH reduction, our economic analysis employs a simplified cost model not capturing market complexities. Fifth, although our 50-kW experimental validation (Section 3.1, Figure 6) confirms simulation predictions within acceptable margins, laboratory-scale testing leaves uncertain whether results transfer to industrial installations (5-50 MW). Finally, the capacity factor improvements reported in Section 3.2 (68.3% vs. 61.2%) assume

perfect hydrogen storage availability and neglect downstream process coupling.These limitations do not invalidate our findings but rather define their current scope and identify critical directions for future work. The demonstrated performance improvements—18.3% efficiency gain, 34.7% thermal cycling reduction, and 12.5% cost reduction—remain significant and practically meaningful within these bounded conditions. The identified gaps provide a clear roadmap for subsequent research phases, particularly industrial-scale pilot studies (5-20 MW) over 6–12-month operational periods currently under development at our institution. Such extended field trials will empirically validate the degradation predictions, assess scale-up viability, and test the control framework under the full complexity of industrial operating conditions including hydrogen demand variability and storage constraints

4. Conclusion

This research successfully developed advanced Model Predictive Control strategies for Power-to-X systems producing green hydrogen from variable renewable energy sources. The hierarchical adaptive MPC framework achieved quantifiable performance improvements over conventional PI control: 18.3% higher production efficiency during high-variability periods (95% CI: 14.7-21.9%), 34.7% reduction in thermal cycling stress, translating to an estimated 22% equipment lifetime extension, and 12.5% reduction in levelized hydrogen cost. These results demonstrate systematic multi-objective optimization—simultaneously maximizing production, minimizing degradation, reducing costs, and providing grid frequency regulation services—within a computationally tractable framework solvable in under 200 milliseconds on industrial embedded controllers. Experimental validation on 50 kW PEM electrolyzer hardware confirmed simulation predictions within 8-12% error margins, with detailed mismatch analysis establishing practical deployment viability. This experimental validation addresses critical gaps in existing literature that predominantly rely on simulation-only assessment. These findings provide a technical foundation and economic justification for industrial-scale Power-to-X implementation, demonstrating that advanced control enables dual-purpose capability essential for future renewable energy systems. Extended field validation at industrial scale (5+ MW) over 6–12-month periods represent the critical next research direction for empirically confirming long-term degradation predictions.

REFERENCES

Abdulwahab, I., Shehu, A., and Taiwo, A. 2021. An improved hybrid micro-grid load frequency control scheme for an autonomous system. FUOYE Journal of Engineering and Technology, 6(4): 382-389. https://doi.org/10.46792/fuoyejet.v6i4.698

Awad, M., Rashed, A., and Radwan, A. 2019. Ultrasound propagation in two-layer gas flow. International Journal of Hydrogen Energy, 44(51): 27596-27608. https://doi.org/10.1016/j.ijhydene.2019.08.192

Bessarabov, D., and Millet, P. 2018. PEM water electrolysis (Vol. 1). Academic Press. https://doi.org/10.1016/B978-0-08-102830-8.00001-1

Bloomberg New Energy Finance. 2024. Hydrogen economy outlook 2024. BNEF Publications.

Bogdanov, D., Gulagi, A., Fasihi, M., and Breyer, C. 2021. Full energy sector transition towards 100% renewable energy supply. Applied Energy, 283, 116273. https://doi.org/10.1016/j.apenergy.2020.116273

Camacho, EF., and Bordons, C. 2013. Model predictive control (2nd ed.). Springer. https://doi.org/10.1007/978-0-85729-398-5

Carmo, M., Fritz, D. L., Mergel, J., and Stolten, D. 2013. A comprehensive review on PEM water electrolysis. International Journal of Hydrogen Energy, 38(12): 4901-4934. https://doi.org/10.1016/j.ijhydene.2013.01.151

Chanderis, M., Médeau, V., Guillet, N., Chelghoum, S., Thoby, D., and Fouda-Onana, F. 2015. Membrane degradation in PEM water electrolyzer. International Journal of Hydrogen Energy, 40(3): 1353-1366. https://doi.org/10.1016/j.ijhydene.2014.11.111

Chen, H., Xuan, J., Zi, G., Zhang, H., and Chen, B. 2021. Optimal scheduling strategy for electrolytic hydrogen storage. Journal of Energy Storage, 33, 102023. https://doi.org/10.1016/j.est.2020.102023

Dahunsi, FM., Abdul-Lateef, OA., Melodi, AO., Ponnle, AA., Sarumi, OA., and Adedeji, KA. 2022. Smart grid systems in Nigeria: Prospects, issues, challenges and way forward. FUOYE Journal of Engineering and Technology, 7(2): 185-200. https://doi.org/10.46792/fuoyejet.v7i2.781

Dörfler, F., Simpson-Porco, JW., and Grammatico, S. 2020. Breaking the hierarchy: Distributed control and economic optimality in microgrids. IEEE Transactions on Control of Network Systems, 7(1): 1-26. https://doi.org/10.1109/TCNS.2020.2973759

Federal Energy Regulatory Commission. 2023. Assessment of ancillary service markets in restructured electricity markets. FERC Report RM22-12-000.

García, P., Torreglosa, JP., Fernández, LM and Jurado, F. 2019. Control strategies for high-power electric vehicles. Expert Systems with Applications, 40(12): 4791-4804. https://doi.org/10.1016/j.eswa.2013.02.028

Götz, M., Lefebvre, J., Mörs, F., McDaniel Koch, A., Graf, F., Bajohr, S., Reimert, R and Kolb, T. 2016. Renewable Power-to-Gas: A technological and economic review. Renewable Energy, 85, 1371-1390. https://doi.org/10.1016/j.renene.2015.07.066

Guilbert, D., Collura, SM and Scipioni, A. 2017. DC/DC converter topologies for electrolyzers. International Journal of Hydrogen Energy, 42(38): 23966-23985. https://doi.org/10.1016/j.ijhydene.2017.07.174

International Energy Agency. 2023. Global hydrogen review 2023. IEA Publications. https://doi.org/10.1787/1e0514c4-en

Koponen, J., Ruuskanen, V., Kosonen, A., Niemela, M and Ahola, J. 2020. Effect of power quality on the design of proton exchange membrane water electrolysis systems. Applied Energy, 279, 115791. https://doi.org/10.1016/j.apenergy.2020.115791

Lettenmeier, P., Wang, R., Abouatallah, R., Helmly, S., Morawietz, T., Hiesgen, R., Kolb, S., Burggraf, F., Kallo, J., Gago, A. S., and Friedrich, K. A. 2016. Durable membrane electrode assemblies for proton exchange membrane electrolyzer systems. Electrochimica Acta, 210: 502-511. https://doi.org/10.1016/j.electacta.2016.04.164

Martín, H., de la Hoz, J., Aliana, A., Coronas, S., and Matas, J. 2020. Analysis of the net metering schemes for PV self-consumption in Denmark. Energies, 13(5): 1121. https://doi.org/10.3390/en13051121

Pham, CV., Escalera-López, D., Mayrhofer, K., Cherevko, S., and Thiele, S. 2021. Essentials of high-performance water electrolyzers. Advanced Energy Materials, 11(44): 2101998. https://doi.org/10.1002/aenm.202101998

Corresponding author's email address: durojaiye.koffa@fulokoja.edu.ng

Renewable Energy Institute. 2024. Global renewable curtailment analysis 2023. REI Technical Report RT-2024-01.

Schill, WP., Pahle, M., and Gambardella, C. 2020. Start-up costs of thermal power plants in markets with increasing shares of variable renewable generation. Nature Energy, 2(6): 17050. https://doi.org/10.1038/nenergy.2017.50

Shen, M., Bennett, N., Ding, Y., and Scott, K. 2019. A concise model for evaluating water electrolysis. International Journal of Hydrogen Energy, 36(22): 14335-14341. https://doi.org/10.1016/j.ijhydene.2011.08.020

Shen, T., Zhang, Y., Hou, C., Lu, T., Xu, Y., Zhou, J., and Fang, Y. 2020. Adaptive model predictive control for water electrolysis systems. International Journal of Hydrogen Energy, 45(41), 21543-21555. https://doi.org/10.1016/j.ijhydene.2020.05.210

Smith, C., Hill, AK., and Torrente-Murciano, L. 2020. Current and future role of Haber-Bosch ammonia in a carbon-free energy landscape. Energy & Environmental Science, 13(2): 331-344. https://doi.org/10.1039/C9EE02873K

Ursúa, A., Gandía, LM., and Sanchis, P. 2012. Hydrogen production from water electrolysis: Current status and future trends. Proceedings of the IEEE, 100(2): 410-426. https://doi.org/10.1109/JPROC.2011.2156750

Vogl, V., Åhman, M. and Nilsson, LJ. 2018. Assessment of hydrogen direct reduction for fossil-free steelmaking. Journal of Cleaner Production, 203, 736-745.

Corresponding author's email address: durojaiye.koffa@fulokoja.edu.ng